Modeling Reactive Geochemical Transport in Natural Fractured Rock Systems Over Geological Time

Tianfu Xu[(1)], Karsten Pruess[(1)], and George Brimhall[(2)]

(1) Earth Sciences Division, Lawrence Berkeley National Laboratory, University of California, Berkeley, CA 94720
(2) Department of Geology and Geophysics, University of California, Berkeley, CA 94720

Abstract. Reactive fluid flow and geochemical transport in natural fractured rock systems has been of increasing interest in the areas of mineral deposits, sedimentary diagenesis, and fluid-rock interactions in hydrothermal systems. Validation of numerical models for natural and anthropogenic systems may differ markedly, relying on quantitative measurements for the former, while often involving qualitative observation for the latter. We have used a reactive geochemical transport simulation tool TOUGHREACT to investigate two natural fractured rock systems: (1) hydrothermal alteration and (2) supergene copper enrichment. The numerical results have been compared with field observed patterns and sequences of mineral alteration. For the problem of mineral alteration, the observed sequence of argillic alteration in Long Valley Caldera (California, USA) is reasonably well reproduced in the numerical simulation. Numerical simulation of simplified supergene enrichment systems which are hydro-chemically differentiated by the vadose zone offers confirmation of well-posed questions based upon field study and petrologic information. The results from the two problems illustrate how by abstraction of a simplified set of relevant factors, certain natural processes can be effectively modeled and how model validity can be tested against qualitative field observations. In addition, the modeling results provide useful insight into process mechanisms such as fracture-matrix interaction, water-gas-rock interaction, and conditions and parameters controlling geochemical evolution.

1. Introduction

Reactive fluid flow and geochemical transport in natural fractured rock systems has been of increasing interest to investigators in the areas of geosciences such as mineral deposits, sedimentary diagenesis, and fluid-rock interactions in hydrothermal systems. Validation of numerical models for natural and anthropogenic (engineered) systems may differ markedly. In anthropogenic systems such as contaminant transport and nuclear waste repositories, models must be validated based on measurements of state variables such as pressure, water saturation, and chemical concentration, and the scientific relevance of modeling must be in prediction. For natural phenomena, the geological relevance of modeling often is in hypothesis testing, because natural processes and geochemical systems may involve many complications and uncertainties to allow for quantitative prediction. Natural mineral systems are characterized by the abundance and distribution of primary and secondary mineral phases, and by the composition of fluid phases (aqueous, gas). Often it is the presence or absence of certain minerals that provides clues to the specific physical and chemical processes and conditions during the evolution of the system. In this sense empirical tests of the accuracy of geochemical modeling are of a more qualitative nature for natural systems. What is important, however, is in constraining numerical

models with boundary and initial conditions derived from integrated observational studies which describe the system in a quantitative petrologic and geochemical manner such that specific, well-posed questions can be answered by numerical results which abstract only the essential features in a vastly simplified domain compared to the realities of nature. It is in this simplification of nature that the real strength of numerical modeling resides. If modeling can find an unambiguous answer to a simple question which is well-posed, then something can be learned. However, the only rigorous test of numerical results is by comparison with known patterns, sequences and processes from natural systems, although they are usually qualitative rather than quantitative in terms of mineral abundances. Therefore, in this paper we use the term "observation" instead of "measurement", and we intend to bridge the gap between observation and modeling.

Methods for modeling geochemical reactions in this complex interplay of physical and chemical transport processes are described in Xu and Pruess (2001b). The physical and chemical process model is embodied in a numerical simulator TOUGHREACT. The simulator was implemented by introducing reactive geochemistry into the framework of the existing non-isothermal multi-phase flow code TOUGH2 (Pruess, 1991). In this paper, we present two examples that use the TOUGHREACT simulator to test geochemical hypotheses based on petrologic observation, and to compare with field observed patterns and sequences of mineral assemblage. The first example is a modeling study on mineral alteration in fractured caprock of magmatic hydrothermal systems. The second is supergene copper enrichment in fractured rock, in which oxygen gas diffusion from the land surface through fractured rock promotes the alteration of the primary sulfide minerals and the subsequent deposition of secondary minerals.

2. Mineral Alteration in Hydrothermal Systems

2.1. Problem setup

The simulation study on mineral alteration in hydrothermal systems uses, as an example, water and gas chemistry data as well as caprock mineral composition from the hydrothermal system in Long Valley Caldera (LVC), California. The LVC is a 450 km^2 elliptical depression located along the eastern front of the Sierra Nevada in east-central California (Sorey, 1985; White and Peterson, 1991; and Sorey et al., 1998). The flow system studied is intended to capture realistic features of fractured magmatic hydrothermal systems of the LVC. Many hot springs in and around LVC occur along north to northwest trending normal faults, and are derived from hydrothermal reservoirs. Hot water is transported upward along fault systems into shallow aquifers (Sorey, 1985; White and Peterson, 1991). In these aquifers, the hydrothermal fluids mix with varying proportions of cold meteoric water before discharging in the hot springs.

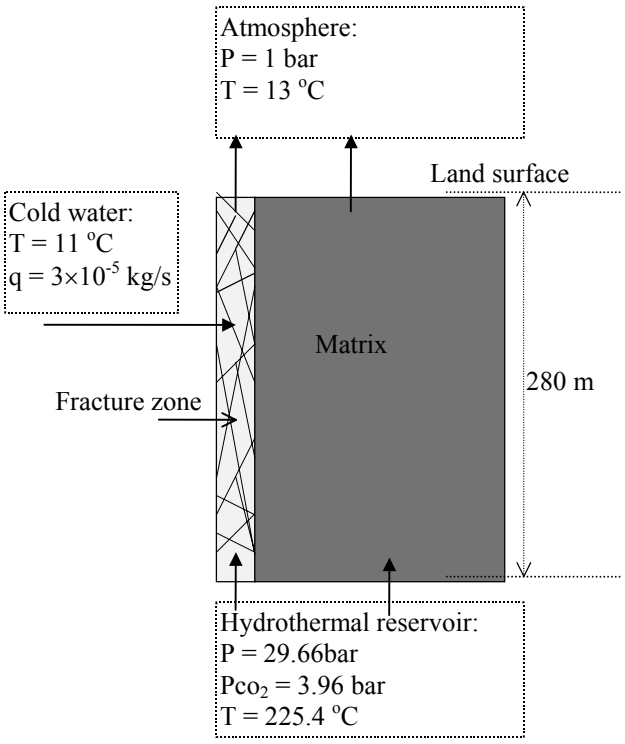

Figure 1. Vertical 2-D section model for hydrothermal fluid flow and rock alteration in a fractured rock.

For the sake of simplification and interpretation of results, we consider an idealized fractured rock with a set of plane, and parallel vertical fracture zones of equal aperture (0.1 m) and spacing (3.5 m). Because of the symmetry of this fractured rock, only one column of matrix blocks needs to be modeled (Figure 1). We simulated a vertical column extending from the atmosphere (top boundary) through the fracture-matrix system (and extending) to the hydrothermal reservoir (bottom boundary). The depth of the hydrothermal reservoir varies from site to site. For example, according to the data presented in White and Peterson (1991) for the LVC, the reservoir depth varies from several tens of meters to near 1000 meters. In this study, we use a single depth of 280 m for simplicity. A 1-m-thick vertical slice is modeled, where a total depth of 280 m is discretized into 56 layers of 5 m thickness. The fracture is considered as one model grid zone. The rock matrix is further discretized into 6 grid zones with permeability and reactive surface area decreasing away from the fracture (Table 1). A thermal conductivity of 2.1 W/m^{o}C, a specific heat of 920 J/kg^{o}C, and an aqueous chemical diffusion coefficient of 1×10^{-10} m^2/s are used. Other parameters for the fracture and matrix are listed in Table 1. The top atmosphere and bottom hydrothermal reservoir boundaries are modeled as constant pressure boundaries with properties shown in Figure 1. At a depth of 87.5 m the rising hot water mixes with the shallow cold meteoric aquifer water. The cold water (11 ^{o}C) recharge is assumed to occur only in the fracture grid block at a rate of 3×10^{-5} kg/s, and is treated as a source term for fluid, heat and chemical constituents, the concentrations of which are given in Table 2.

Table 1. Some parameters used in the simulation for the fracture-matrix system

medium	Fracture zone	matrix	matrix	matrix
symbol	F	M1	M2	M3, M4, M5, M6
grid spacing (m)	0.05	0.1	0.15	0.2, 0.3, 0.4, 0.55
permeability (m^2)	1×10^{-12}	1×10^{-14}	1×10^{-15}	1×10^{-16}
parameters for relative permeability and capillary pressure functions (*van Genuchten*, 1980):				
λ	0.457	0.457	0.457	0.457
S_{lr}	0.15	0.20	0.30	0.40
S_{ls}	1.0	1.0	1.0	1.0
P_0(Pa)	6.195×10^3	6.195×10^4	1.959×10^5	6.195×10^5
porosity	0.5	0.1	0.09	0.08
reactive surface reduction factor	1	0.8	0.4	0.2

The reservoir chemical composition is based on data reported by White and Peterson (1991). The concentrations of major chemical species in samples at various wells are in general similar, and we arbitrarily choose data from well RDO-8 (Table 2) for our simulation. CO_2 is the dominant gaseous species in the hydrothermal system, and its partial pressures range from 1 to 9 bar (1 bar ≡ 10^5 Pa) . We use an intermediate partial pressure value of approximately 4 bars. The cold recharge water chemical composition is taken from Sorey (1985) for cold Big Springs of LVC (Table 2) which is assumed to be representative of the shallow aquifer meteoric water.

Table 2. Aqueous chemical concentrations (mol/kg H_2O) of hot reservoir water and cold meteoric water used for the simulation study.

Component	hot water	cold water
Ca^{2+}	$4.49\text{x}10^{-4}$	$1.27\text{x}10^{-4}$
Mg^{2+}	$1.44\text{x}10^{-5}$	$2.43\text{x}10^{-4}$
Na^{+}	$1.65\text{x}10^{-2}$	$1.00\text{x}10^{-3}$
K^{+}	$1.23\text{x}10^{-3}$	$1.00\text{x}10^{-4}$
HCO_3^{-}	$7.92\text{x}10^{-3}$	$1.21\text{x}10^{-3}$
SO_4^{2-}	$1.86\text{x}10^{-3}$	$8.33\text{x}10^{-5}$
Al^{3+}	$1.00\text{x}10^{-6}$	$1.00\text{x}10^{-6}$
SiO_2(aq)	$4.61\text{x}10^{-3}$	$9.65\text{x}10^{-4}$
Cl^{-}	$7.41\text{x}10^{-3}$	$1.61\text{x}10^{-4}$
pH	6.6	6.8
T (^{o}C)	225	11

Flexser (1991) reported on hydrothermal alteration in six western moat drillcores in the Long Valley Caldera. Mineral phases were identified by X-ray diffraction analysis of both bulk samples and clay separates, supplemented by examination of thin sections. The following phases were observed: glass, quartz, feldspar, cristobalite-α or opal-CT, kaolinite, smectite, illite, chlorite, and calcite. The mineralogy observed represents the present mineral assemblage after alteration processes. For the modeling study, we require the assemblage prior to the beginning of the argillic alteration. We assume initially glass, quartz, feldspar, cristobalite-α (or opal-CT) are present. We used K-feldspar, albite, and anorthite to substitute feldspar that is a solid solution. The abundance of primary minerals used in the simulation is listed in Table 3. The secondary

phases in TOUGHREACT were specified based on those identified from the drillcores (Flexser, 1991), which is also listed in Table 3. We used Na-, Ca-, K-, and Mg-smectite to represent the solid solution smectite. Chlorite was substituted using clinochlore-14a. We neglected zeolite minerals in the simulation because they occur only locally in slight amounts in the LVC, even though they usually are constituents in hydrothermally altered rocks. Thermodynamic data for other minerals were taken from the EQ3/6 V7.2b database (Wolery, 1992) which were derived using SUPCRT92 (Johnson et al., 1992).

Table 3. List of initial caprock mineral volume fractions (in terms of solid), possible secondary mineral phases, and their kinetic properties.

Mineral	Volume (%)	Surface area (m^2/dm^3 medium)	Kinetic constant at 25 ^oC (moles $m^{-2}s^{-1}$)	activation energy (E_a), (KJ/mol)	Reference
Primary:					
glass	40	0.040	$3.16x10^{-13}$	69.08	set to cristobalite-α
quartz	28	0.028	$4.30x10^{-14}$	75.00	Tester et al. (1994)
cristobalite-α	8	0.008	$3.16x10^{-13}$	69.08	Renders et al. (1995)
K-feldspar	18	0.018	$1.00x10^{-12}$	67.83	Blum and Stillings (1995)
albite	3	0.003	$1.00x10^{-12}$	67.83	set to K-feldspar
anorthite	3	0.003	$1.00x10^{-12}$	67.83	set to K-feldspar
Secondary:					
calcite	0	0.01	$1.60x10^{-9}$	41.87	Svensson and Dreybrodt (1992)
clinochlore-14a	0	0.01	$1.00x10^{-14}$	58.62	set to illite
kaolinite	0	0.01	$1.00x10^{-13}$	62.76	Nagy (1995)
illite	0	0.01	$1.00x10^{-14}$	58.58	Knauss and Wolery (1989)
smectite-Na	0	0.01	$1.00x10^{-14}$	58.62	set to illite
smectite-Ca	0	0.01	$1.00x10^{-14}$	58.62	set to illite
smectite-K	0	0.01	$1.00x10^{-14}$	58.62	set to illite
smectite-Mg	0	0.01	$1.00x10^{-14}$	58.62	set to illite

Mineral dissolution and precipitation proceeds subject to kinetic constraints. A first order kinetic rate law was used (Steefel and Lasaga, 1994). The kinetic constants at 25 ^oC and activation energies are also given in Table 3. The reactive surface area evolution in natural geologic media is very complex. In this study, we simply used a total initial reactive surface area of 0.1 m^2 per dm^3 (cubic decimeter) medium. The initial area for each primary mineral is calculated by multiplying the total surface area with its volume fraction, which is also listed in Table 3. The initial reactive surface areas given in Table 3 must be multiplied by the reactive surface area factor given in Table 1 for each different matrix grid zone, in order to take into account the fact that reactive surface areas may decrease from the fractures towards the interior of the rock matrix. The precipitation of possible secondary minerals (also given in Table 3) is represented using the same kinetic expression as that for dissolution. To simplify the description of precipitation kinetics, a constant reactive surface area of 0.01 m^2 per dm^3 (cubic decimeter) medium is used for the entire simulation time. Kinetic rates of precipitation depend on the activities of reactants supplied by dissolution.

The simulation is run for 20,000 years. Initially, we limit the simulation only to fluid and heat flow until a steady-state is attained. Then we simulate chemical transport and fluid-rock interactions using the steady-state fluid and heat flow as the initial condition.

2.2. Results

Figure 2 gives a distribution along the vertical fracture zone obtained from a steady-state fluid and heat flow simulation. The liquid saturation (Figure 2a) decreases slightly with increasing elevation until a depth of 87.5 m, where it increases dramatically due to the cold water recharge. It then again decreases slightly, and finally liquid saturation increases at the top. The relative liquid flow rate (R_l) normalized to the total (fracture and matrix) land surface discharge (5.49×10^{-5} kg/s), slightly decreases from the bottom like the liquid saturation. After the cold water recharge R_l dramatically increases from 24% to 87%. Finally 80% of the liquid discharge is from the narrow fracture at the land surface. Nearly all of the total CO_2 output (2.46×10^{-6} kg/s) discharges from the fracture. In general, total gas pressure P_g (CO_2 and vapor) gradually decreases from the bottom to the top (Figure 2b). CO_2 partial pressure P_{CO_2} generally also decreases from the bottom to the top but a peak value appears after mixing with cold water. This is because (1) gas phase saturation is dramatically decreased due to the cold water recharge, (2) cooling and condensation causes CO_2 to become the dominant gas phase constituent, (3) CO_2 solubility in water has a minimum at 160 ^oC (Battistelli et al., 1997), the temperature in the mixing zone, and (4) it is assumed the mixing occurs at one narrow location. Temperature gradually falls with elevation (Figure 2c), then drops suddenly when mixing with the cold water (11 ^oC) occurs. Close to the land surface temperature decreases very rapidly due to heat loss to the atmosphere. More results on fluid flow is given in Xu and Pruess (2001a)

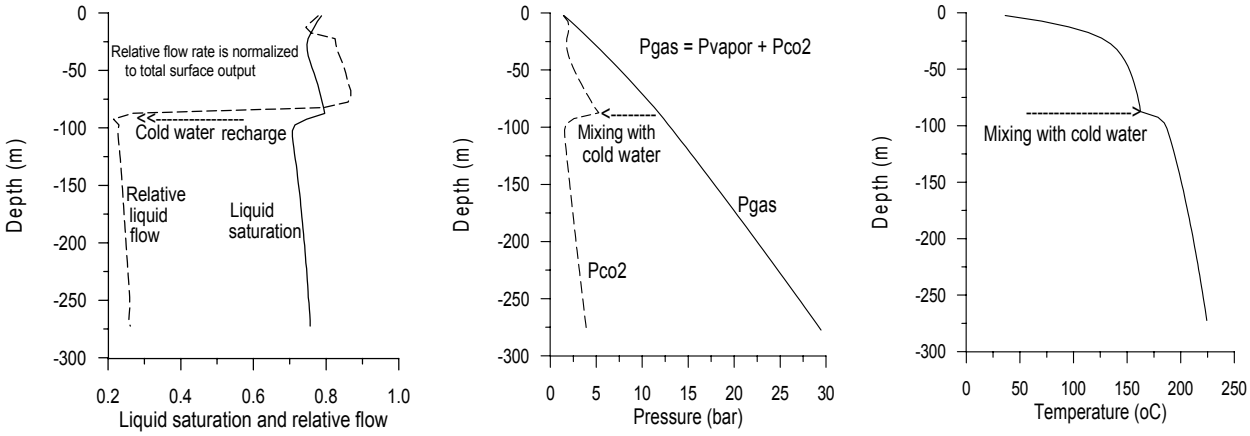

Figure 2. Steady-state distribution of liquid saturation (a), gas pressure (b), and temperature (c) distribution along the fracture zone.

We express simulated mineral abundances as volume percentage in terms of the bulk medium. We begin by examining the evolution of the primary minerals. Dissolution of glass (Figure 3a), cristobalite-α (Figure 3b), and quartz generally decrease from the bottom heat source to the top land surface with decreasing temperature. After mixing with cold meteoric water, their dissolution decreases significantly. Glass dissolution is more extensive from the fracture to the interior of the rock matrix. Cristobalite-α dissolution is also considerable and its pattern is similar to that of glass. Quartz dissolution mostly occurs along the fracture. After

20,000 years, glass and cristobalite-α have been removed from most of the fracture, while significant amounts of quartz still remain. Albite (Figure 3c) is extensively dissolved in the entire fracture and in the top of the rock matrix. K-feldspar dissolution occurs mostly at the top of the fracture. Anorthite (Ca-feldspar) dissolution mainly occurs (1) close to the heat source due to calcite precipitation and (2) after the mixing due to Ca-smectite precipitation.

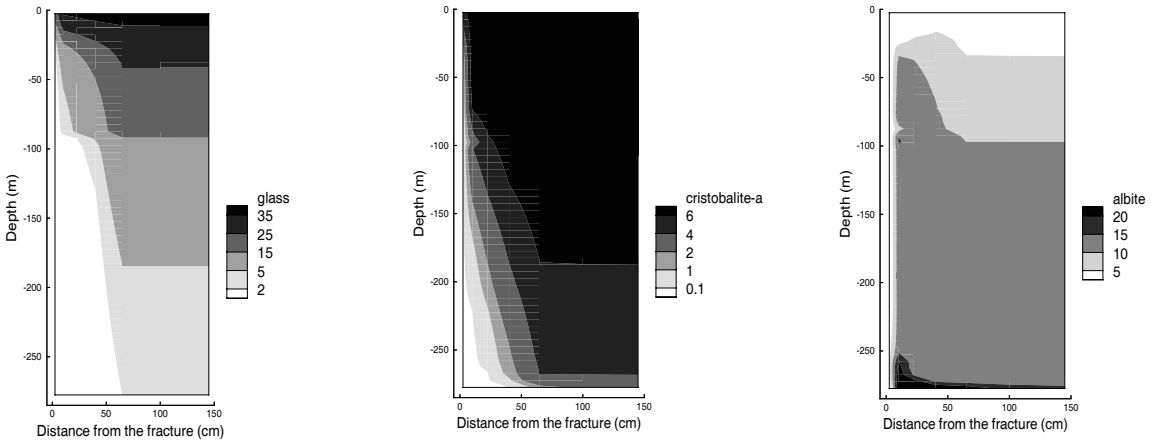

(a) (b) (c)

Figure 3. Abundance (in volume %) of the primary minerals after 20,000 years.

Now we turn to the formation of secondary mineral phases. Ca^{2+} released from dissolution of anorthite is taken up by calcite precipitation (Figure 4a). Calcite precipitation occurs only close to the bottom heat source, because calcite solubility increases with decreasing temperature. The precipitation occurs mainly in the fracture, and gradually decreases away from the fracture in the matrix interior. Clinochlore-14 (a chlorite mineral) precipitation pattern (Figures 4b) is similar to that of calcite. Kaolinite precipitation occurs in the lower temperature region (Figure 4c). Illite is formed extensively except near the top (Figure 4d). Smectite minerals are formed in the lower temperature region above the mixing horizon. Formation of Na- and Ca-smectite is extensive (Figures 4e and f), and that of K- and Mg-smectite is concentrated in and close to the fracture.

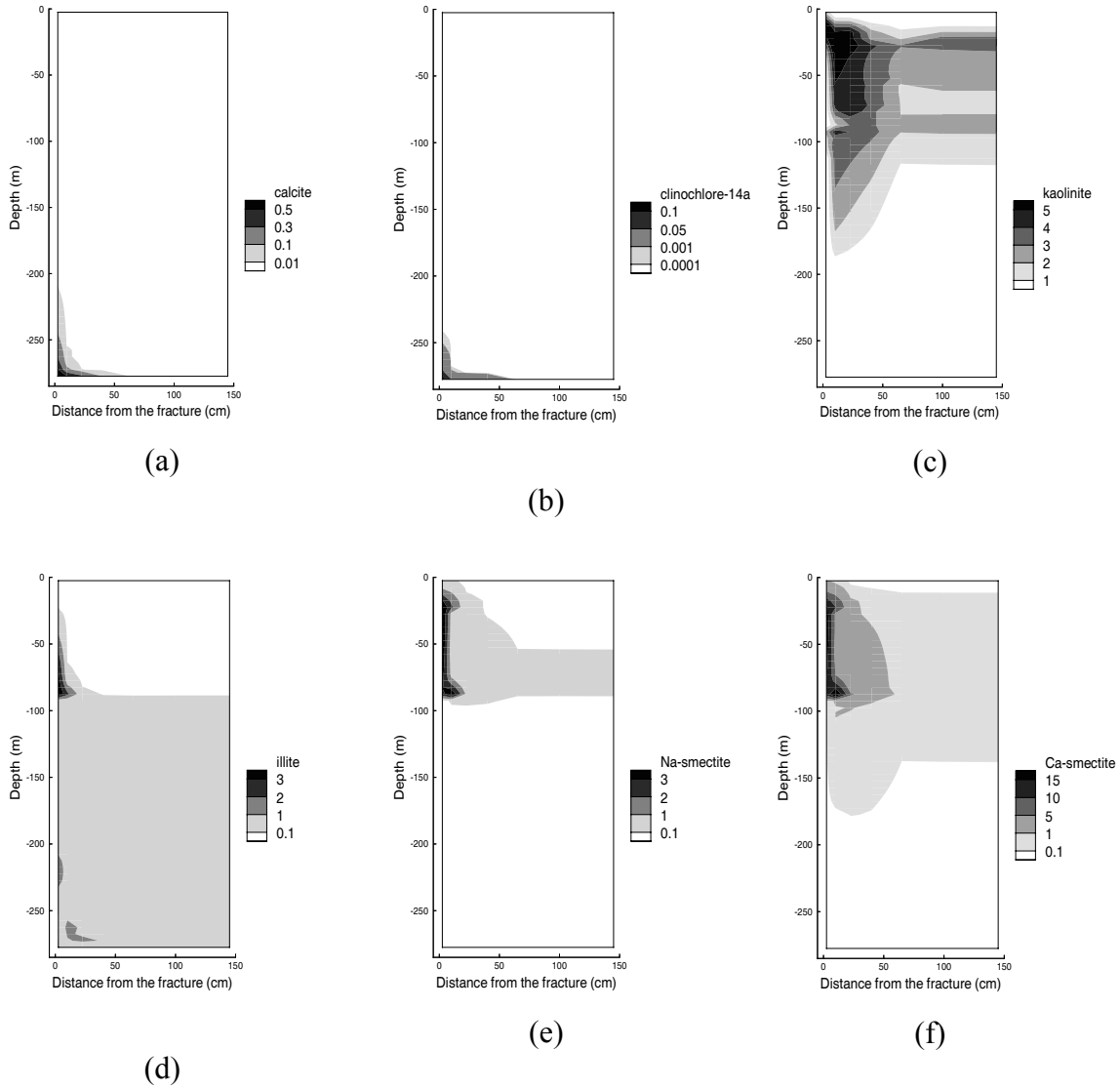

Figure 4. Abundance (in volume %) of the secondary minerals after 20,000 years.

2.3. Comparison with observations

The simulated pattern of argillic alteration of silicic rocks is generally consistent with the observations reported by Flexser (1991) for six western moat drillcores in the LVC. The observed three-part zonation of the distribution of clay minerals is reasonably well reproduced by the simulation. The upper argillic zone, at the lower temperature region after the mixing, is characterized by kaolinite (Figure 4c) and smectite (Figures 4e and f) alteration. The simulated upper alteration pattern is consistent with the field observations (Flexser, 1991). Unalterated glass (Figure 3a), quartz, and K-feldspar remain close to the land surface, which also agrees with the observations.

In the lower argillic zone, illite (Figure 4d) is the sole clay alteration phase, and kaolinite and smectite are absent, which agrees with the observations. Cristobalite is also absent there or

reduced to trace amounts according to the core observations. In the simulation cristobalite is dissolved completely in the fracture but some remains in the interior of the rock matrix (Figure 3b). The simulated calcite precipitation (Figure 4a) in the high temperature fracture region is consistent with field observations. As reported by Flexser (1991), many of the fractures are open and are typically filled with calcite, and sometimes illite. Calcite precipitation in the fracture may inhibit fluid flow and chemical transport, and stop fracture fluid and chemical exchange with the matrix. These effects are not considered in the present simulation. In the lower zone, chlorite (substituted by clinochlore-14, Figure 4b) is precipitated with a similar pattern to that of calcite, also in agreement with Flexser's observation.

Between and overlapping the upper and lower argillic zones, mixed illite and smectite are observed. In the simulation, illite precipitation occurs from the bottom to the mixing horizon. A larger amount of illite is found in the mixing horizon. This may be caused by a higher concentration of Mg from the cold water used in the simulation (Table 2). Ca-smectite (Figure 4f) precipitation extends below the mixing horizon, even though other smectite minerals only occur above the mixing horizon. This reflects the existence of an intermediate mixed illite and smectite zone in the simulation.

3. Supergene copper enrichment

3.1. Problem setup

Supergene copper enrichment (SCE) involves hydrochemical differentiation by near-surface weathering processes in which water transports metals from a source region or leached zone (Ague and Brimhall, 1989) to a locus of an enrichment blanket zone where these ions are reprecipitated as secondary ore compounds conserving mass (Figure 5). Oxidative weathering of pyrite (FeS_2) and chalcopyrite ($CuFeS_2$) causes acidification and mobilization of metals in the oxidizing zone and intense alteration of primary minerals, with subsequent formation of enriched secondary copper bearing sulfide mineral deposits (enrichment blanket) in the reducing conditions below the water table. Such oxidative weathering driven processes have produced some of the world's largest copper deposits (Ague and Brimhall, 1989). The present investigation on geochemical transport in SCE systems is not specific to any field site, but the geochemistry for this work was based on field and laboratory studies of SCE systems as carried out by Brimhall, Alpers, and Cunningham (1985), and Ague and Brimhall (1989). The SCE processes typically took place in a fractured porous medium such as El Salvador, Chile (Mote and Brimhall, 1999). To gain better insight into the processes involved, we simulated two cases, (1) a one-dimensional unsaturated-saturated porous medium flow and (2) a fractured rock system. Here we only present the SCE process in the fractured rock system. Results of the 1-D porous medium case are given in Xu et al. (2001). The study of the fractured rock provides a more detailed picture of the SCE processes on a smaller scale, while the homogeneous porous medium study gives a general pattern of the SCE on a large scale.

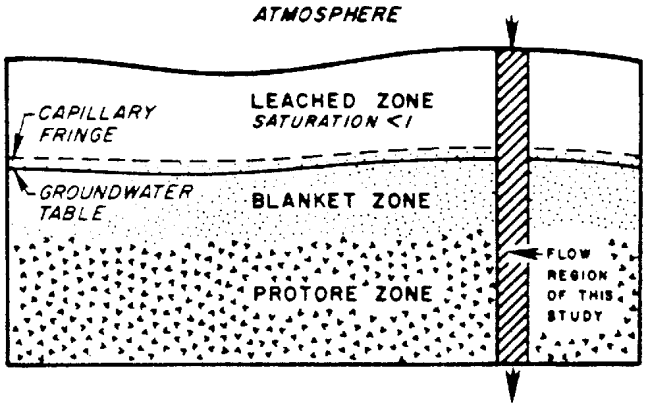

Figure 5. A schematic representation of a supergene copper enrichment system according to Ague and Brimhall (1989).

The method of "multiple interacting continua" (MINC) is used to resolve “global” flow and diffusion of chemicals in the fractured rock and its interaction with “local” exchange between fracture and matrix rock. This method was developed by Pruess and Narasimhan (1985) for fluid and heat flow in fractured porous media. The extension of the MINC method to reactive geochemical transport is described in detail by Xu and Pruess (2001b). It is well-known that in the case of reactive chemistry diffusive fluxes may be controlled by reactions occurring near (within millimeters) the fracture walls. The resolution of concentration gradients in matrix blocks is achieved by appropriate subgridding. The MINC concept is based on the notion that changes in fluid pressures and chemical concentrations propagate rapidly through the fracture system, while invading the tight matrix blocks only slowly. Therefore, changes in matrix conditions will be (locally) controlled by the distance from the fractures and can then be modeled by means of one-dimensional strings of nested grid blocks (Figure. 6).

We consider an idealized fractured porous medium with two perpendicular sets of plane, parallel vertical fractures of equal aperture and spacing. Because of symmetry only one column of matrix blocks needs to be modeled. Figure 6 shows an areal view of a rock matrix column that is surrounded by vertical fractures with a spacing of 0.5 m, with subgridding of the matrix according to the MINC method. Subgrid 1 represents the fracture domain which is defined to include 50 percent by volume of wall rock. Subgrids 2 through 7 represent the rock matrix. In the vertical direction, a total of 10 grid block zones are used with a spacing of 2 m. A net rainwater infiltration rate of 0.015 m y^{-1} over the entire area was applied to the fractures. Water pressure is held constant at 2 bar at the bottom (z = -20 m), so that the water table is located at a depth of 10 m. In addition to global water flow and chemical transport in the fracture network, our model considers flow and transport between fractures and matrix, as well as vertical matrix-matrix water flow and chemical transport. The steady-state water saturations obtained without chemical reactions are used as initial conditions for the calculation of reactive geochemical transport. Hydrological parameters used for the fracture and matrix are given in Xu et al (2001).

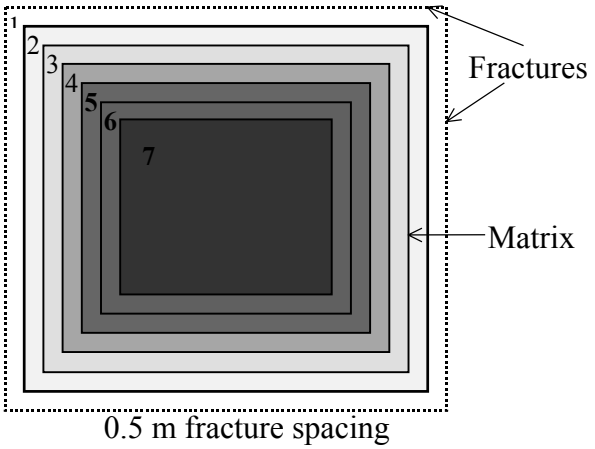

Figure 6. Subgridding of a rock matrix in the method of "multiple interacting continua" (MINC). The figure represents an areal view of a rock matrix column that is surrounded by vertical fractures.

The geochemical transport simulation considers unsaturated-saturated liquid phase flow and diffusive supply of oxygen to the protore. Oxygen is treated as an ideal gas, and its interaction with the aqueous solution is assumed at equilibrium. The oxygen partial pressure at the land surface boundary is assumed to be constant at 0.2 bar. The rock matrix is initially filled entirely with a protore mineral assemblage (pyrite, chalcopyrite, magnetite, k-feldspar, albite, anorthite, annite, muscovite, quartz, anhydrite). The secondary minerals considered are covellite, chalcocite, bornite, goethite, hematite, kaolinite, alunite, and amorphous silica. Mineral dissolution and precipitation were considered to be kinetically-controlled, and a first order kinetic rate law was used. Details on geochemical conditions and parameters are given in Xu et al. (2001).

3.2. Results

The simulation results indicate that the tight rock matrix has strong capillary suction and is almost water saturated, while the fractures in the unsaturated zone have a water saturation of 0.3. Most pores in the unsaturated fractures are filled with gas phase, which provides an oxygen diffusion path from the land surface. The water entering the fractures at the land surface boundary is imbibed into the rock matrix, reducing flow in the fractures to less than 20 percent of the total infiltration over 5 m depth (Figure 7). Then the water taken up by the matrix is released to the fractures just above the water table (at z = -10 m). In the saturated zone, almost all water flows through the fractures since the saturated permeability of the fractures is four orders of magnitude greater than that of the matrix.

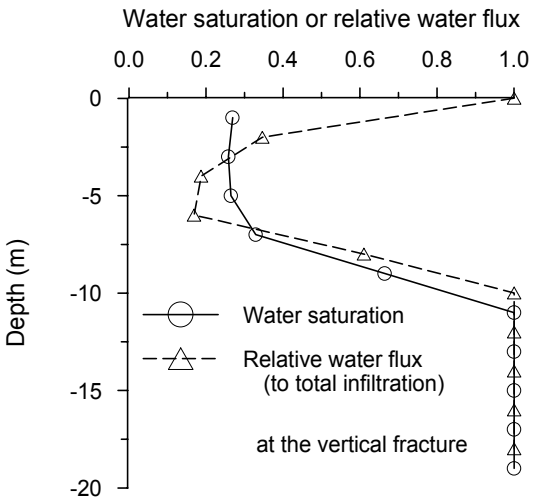

Figure 7. Steady-state water saturation and relative water flux (to total infiltration) passed through the fractures

Pyrite and chalcopyrite oxidative dissolution takes place mostly in close proximity to the unsaturated fracture zone (Figure 8a and b). Away from the fracture zone, dissolution rates decrease due to limited oxygen access. The oxygen is supplied to the rock matrix partly advectively, dissolved in water, and partly by aqueous and gaseous diffusion. Oxidative dissolution is seen to also occur in the top part of the saturated fracture zone. Other minerals such as k-feldspar (Figure 8c) dissolution follows a similar pattern as pyrite and chalcopyrite dissolution.

Chalcocite precipitation occurs mostly in the fracture just below the water table (Figure 8d), but some also occurs in the matrix just above as well as below the water table. Although changes in mineral abundance are smaller in the matrix, the volume throughout which these changes occur is considerably larger than in the fractures, so that in terms of overall mineral inventory matrix dissolution and precipitation could be very significant. Most covellite precipitates in the deep fracture below the chalcocite precipitation peak (Figure 8e), and a minor amount precipitates in the matrix just above the water table. Most amorphous silica precipitation occurs in the fractures (Figure 8f). The aqueous and gaseous diffusion processes play an important role in the formation of secondary minerals in the matrix. The small aqueous diffusion coefficient is still significant because water advection is slow with an infiltration rate of 0.015 m yr^{-1}.

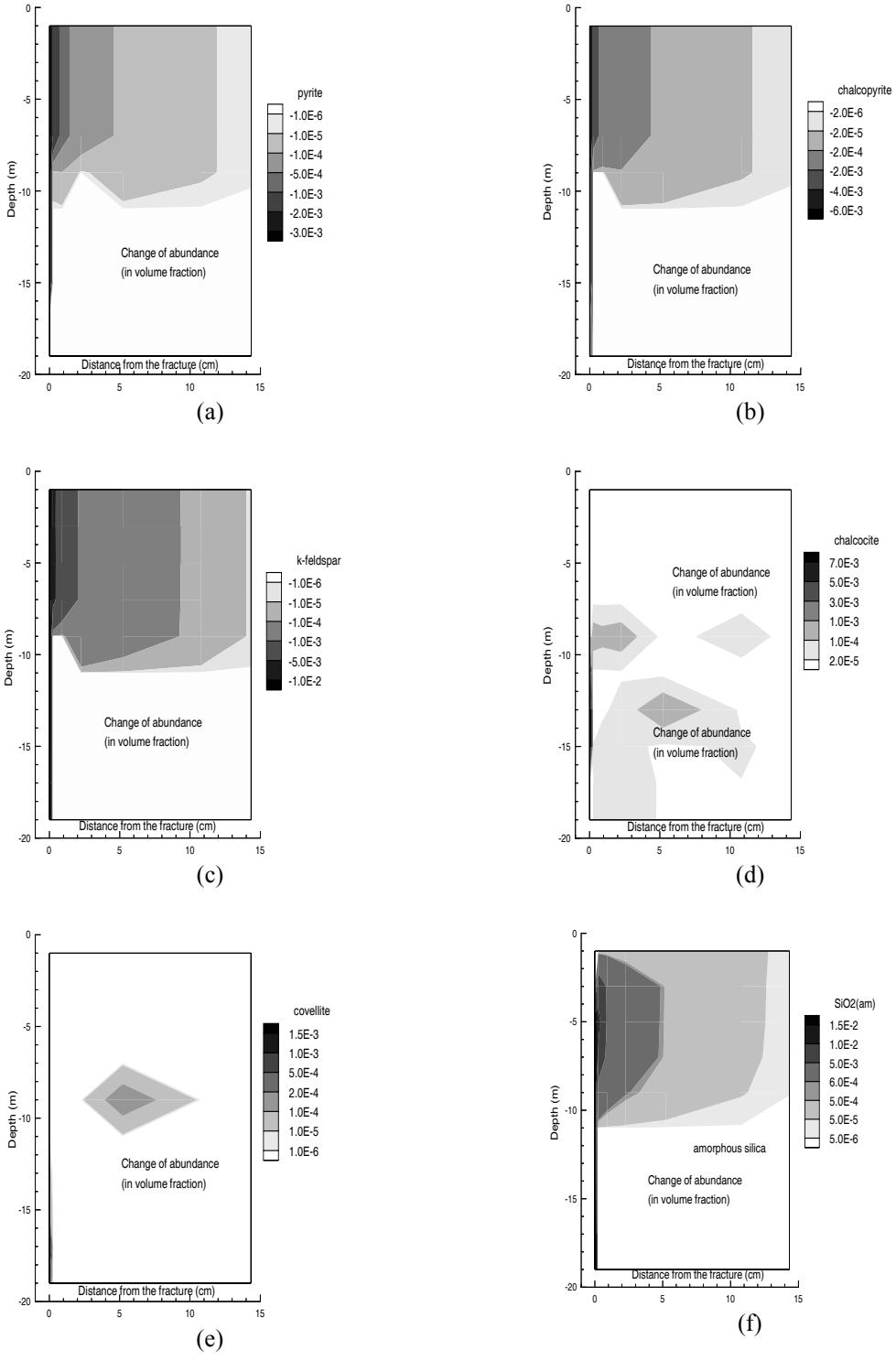

Figure 8. Change of mineral abundance (positive values indicate precipitation and negative dissolution) after 20,000 yrs in the fractured rock.

3.3. Comparison with observation

The alteration of the primary minerals and development of secondary mineral assemblages simulated by our model agree with observations in supergene copper deposits (Ague and Brimhall, 1989). The simulation results are consistent in general with known mineral sequences and spatial and temporal patterns observed in nature. De-stabilization of primary sulfide (pyrite and chalcopyrite) is what drives supergene enrichment. Both of these minerals were found to dissolve in the simulation. Similarly, the wall rock mineral buffer assemblages which resist changes in solution composition were destroyed. Most importantly, the redox buffer (annite-magnetite-orthoclase) was destroyed, thereby allowing the unsaturated part of the systems to oxidize as sulfides were de-stabilized.

It has long been recognized that supergene enrichment is not due to a single stand of the paleo-ground water table but rather to a long-term process of downward accumulation of metals (Locke, 1926) over geological time periods as progressively lower positions within the protore are subjected to oxidation. Enrichment is accomplished by many stages of ground water table descent through a paleo-hydrological evolution (Alpers and Brimhall, 1989), enhanced in certain regions of the earth by climatic change to more arid conditions (Alpers and Brimhall, 1988). Ultimately, where hyperarid conditions eventually occur, such as in the Atacama desert of Chile, insufficient water is available for supergene processes to proceed and enrichment ceases. Similarly with less rainfall, the erosion rate also declines and ideal conditions for preservation of enriched ore deposits are attained. Our 1-D modeling results (Xu et al., 2001), though drastically simplified compared to these effects of nature, do in fact show that with lowering of the ground water table, the leached zone advances downward and previously-precipitated chalcocite and covellite are leached with their constituent copper ions contributing to the development of a lower stand of the enrichment blanket. In addition, the simulation results suggest the migration rate of the enrichment blanket decreases gradually with depth.

4. Conclusions

We have used a reactive transport simulation tool TOUGHREACT to investigate two natural fractured rock systems: (1) hydrothermal alteration and (2) supergene copper enrichment. The numerical results have been compared with field observed pattern and sequences of mineral alteration, which are qualitative rather than quantitative in terms of mineral abundances. For the problem of mineral alteration in fractured caprock of magmatic hydrothermal systems, the observed sequence of argillic alteration in the LVC consists of an upper zone with smectite and kaolinite (in the lower temperature region), a lower illite zone, and an intermediate mixed illite and smectite zone. The sequence is reasonably well reproduced in the numerical simulation. In addition, calcite and chlorite precipitation in the hot region coincides with the observations. Numerical simulation of simplified supergene enrichment systems which are hydro-chemically differentiated by the vadose zone can offer confirmation of well-posed questions based upon field study and petrologic information. Specifically, it has been possible here to demonstrate that oxidation of primary pyrite and chalcopyrite drives supergene leaching and destroys wall rock mineral solution buffer assemblages which otherwise restrain redox conditions to a reducing level. The results from the two problems have illustrated how by abstraction of a simplified set of relevant factors, certain natural processes can be effectively modeled and how model validity can be tested against qualitative field observations. In addition, our “numerical experiments” give a detailed view of the dynamical interplay between coupled hydrologic, thermal, and chemical processes. The modeling results can provide useful insight into process mechanisms

such as fracture-matrix interaction, water-gas-rock interaction, and conditions and parameters controlling geochemical evolution.

Acknowledgement. We thank Patrick Dobson and Keni Zhang for a review of the manuscript and suggestions for improvement**.** This work was supported by the Laboratory Directed Research and Development Program of the Ernest Orlando Lawrence Berkeley National Laboratory, and by the Assistant Secretary for Energy Efficiency and Renewable Energy, Office of Geothermal and Wind Technologies, of the U.S. Department of Energy, under Contract No. DE-AC03-76SF00098.

References

Ague, J. J., and G. H. Brimhall, Geochemical modeling of steady state and chemical reaction during supergene enrichment of porphyry copper deposits, *Economic Geology*, v. 84, p. 506-528, 1989.

Alpers, C. A., and G. H. Brimhall, 1988, Middle Miocene climatic change in the Atacama Desert, northern Chile: Evidence from supergene mineralization at La Escondida, American Geological Society, v. 100, p.1640-1655, 1988.

Alpers, C. A., and G. H. Brimhall, 1989, Paleohydrologic evolution and geochemical dynamics of cumulative supergene metal enrichment at La Escondida, Atacam Desert, Northern Chile, *Economic Geology*, v. 84, p. 229-255, 1989.

Battistelli, A., C. Calore, and K. Pruess, The simulator TOUGH2/EWASG for modeling geothermal reservoirs with brines and non-condensible gas, *Geothermics*, 26, 437-464, 1997.

Blum, A. E., and L. L. Stillings, Feldspar dissolution kinetics, Chapter 7 of chemical weathering rates of silicate minerals, edited by A. F. White, and S. L. Brantley, *Mineral Society of America*, 31, 291–351, Washington D. C., 1995.

Brimhall, G. H., C. N. Alpers, and A. B. Cunningham, Analysis of supergene ore-forming processes and ground water solute transport using mass balance principles: Economic Geology, v. 80, p. 1227-1256, 1985.

DePaolo, D. J., Isotopic effects in dual-porosity fluid-rock systems, In: Proceedings of International Symposium on Dynamics of Fluids in Fractured Rocks: Lawrence Berkeley National Report LBNL-42718, Berkeley, California, 1999.

Flexser, S., Hydrothermal alteration and past and present thermal regimes in the western moat of Long Valley Cadera (California), *J. Volcanol. and Geotherm. Res*., 48, 303-318, 1991.

Johnson, J. W., E. H. Oelkers, and H. C. Helgeson, SUPCRT92: A software package for calculating the standard molal thermodynamic properties of minerals, gases, aqueous species, and reactions from 1 to 5000 bars and 0 to 1000 degrees C, *Computers and Geosciences*, 18, 899–947, 1992.

Knauss, K. G., and T. J. Wolery, Muscovite dissolution kinetics as a function of pH and time at 70°C, *Geochim. Cosmochim. Acta*, 53, 1493–1501, 1989.

Locke, A., Leached outcrops as guides to copper ores, Baltimore, Williams Wilkins Co., 166 p., 1962.

Mote, T. I, and G. H. Brimhall, Mass balance analysis of exotic ore-forming processes and lateral copper transport into the drainage networks of the El Salvador porphyry copper deposit, Chile and its application to discovery of the new exotic mineralization in Quebrada Turquesa: Economic Geology, in press, 1999.

Nagy, K. L., Dissolution and precipitation kinetics of sheet silicates, *Chemical Weathering Rates of Silicate Minerals,* 31, 291–351, 1995.

Pruess, K., and T. N. Narasimhan, A practical method for modeling fluid and heat flow in fractured porous media: *Society of Petroleum Engineers Journal*, v. 25, (1), p. 14-26, 1985.

Pruess, K., TOUGH2: A general numerical simulator for multiphase fluid and heat flow, Lawrence Berkeley Laboratory Report LBL-29400, Berkeley, California, 37 pp., 1991.

Renders, P. J. N., C. H. Gammons, and H. L. Barnes, Precipitation and dissolution rate constants for cristobalite from 150 to 300°C, *Geochim. Cosmochim. Acta*, 59, 1, 77–85. Amsterdam, The Netherlands, Elsevier Science, 1995.

Sorey, M. L., Evolution and present state of the hydrothermal system in Long Valley Cadera, *J. Geophys. Res*., 90, 11219-11228, 1985.

Sorey, M. L; W. C. Evans, B. M. Kennedy, C. D. Farrar, L. J. Hainsworth, and B. Hausback, Carbon dioxide and helium emissions from a reservoir of magmatic gas beneath Mammoth Mountain (California), *J. Geophys. Res*., 103, 15303-15323, 1998.

Steefel, C. I., and A. C. Lasaga, A coupled model for transport of multiple chemical species and kinetic precipitation/dissolution reactions with applications to reactive flow in single phase hydrothermal system, *Am. J. Sci.*, 294, 529-592, 1994.

Svensson, U., and W. Dreybrodt, Dissolution kinetics of natural calcite minerals in CO_2-water systems approaching calcite equilibrium, *Chemical Geology*, 100, 129–145, Amsterdam, The Netherlands, Elsevier Science, 1992.

Tester, J. W., G. W. Worley, B. A. Robinson, C. O. Grigsby, and J. L. Feerer, Correlating quartz dissolution kinetics in pure water from 25° to 625 °C, *Geochim. Cosmochim. Acta*, 58, 2407–2420, 1994.

van Genuchten, M. T., A closed-form equation for predicting the hydraulic conductivity of unsaturated soils, *Soil Sci. Soc. Am. J*., 44, 892-898, 1980.

White, A. F., and M. L. Peterson, Chemical equilibrium and mass balance relationships associated with Long Valley hydrothermal system, California, USA, *J. Volcanol. and Geotherm. Res*., 48, 283-302, 1991.

Wolery, T. J., EQ3/6: Software package for geochemical modeling of aqueous systems: Package overview and installation guide (version 7.0), Lawrence Livermore National Laboratory Report UCRL-MA-110662 PT I, Livermore, California, 1992.

Xu, T., and K. Pruess, On fluid flow and mineral alteration in fractured caprock of magmatic hydrothermal systems, Journal of geophysical Research, v. 106 (B2), 2121-2138, 2001a.

Xu, T., and K. Pruess, Modeling multiphase non-isothermal fluid flow and reactive geochemical transport in variably saturated fractured rocks: 1. Methodology, *American Journal of Science*, v. 301, 16-33, 2001b.

Xu, T., E. Sonnenthal, N. Spycher, K. Pruess, G. Brimhall, and J. Apps, 2001, Modeling multiphase non-isothermal fluid flow and reactive geochemical transport in variably saturated fractured rocks: 2. Applications to supergene copper enrichment and hydrothermal flows, *American Journal of Science*, v. 301, 34-59, 2001.